

Lasers in Manufacturing Conference 2021

The effect of chemical components on wettability at ps laser micromachined surface on stainless steel 304

Munehiro Chijiwa^{a,*}, Niklas Berger^a, Mareike Schäfer^a, Rolf Merz^b, Michael Kopnarski^b, Peter Mitschang^c, Johannes A. L'huillier^a

^aPhotonik-Zentrum Kaiserslautern e.V., 67633 Kaiserslautern, Germany and Research Center OPTIMAS, TU Kaiserslautern, 67663 Kaiserslautern, Germany

^bInstitute of Surface and Thin Film Analytics, IFOS, Research Center OPTIMAS, TU Kaiserslautern, 67663 Kaiserslautern, Germany
^cIVW—Leibniz-Institut für Verbundwerkstoffe GmbH, Manufacturing Science, 67663 Kaiserslautern, Germany

Abstract

Recently, controlling the wettability of metallic surfaces by laser micromachining has become important for many technical applications. However, there is still a challenge in understanding chemical effects on contact angle (CA) since there is even a big gap in knowledge of the laser micromachining's influence on surface chemistry. In this study, the relationship between the local surface chemistry at ps-laser micromachined surfaces on stainless steel 304 and CA was discussed by using a new model description, based on a multiple regression analysis. The proposed model was verified by using the experimental wetting behavior of different kinds of liquid and surface chemistry, characterized by XPS spectroscopy. To have a variety of different wettability of the samples, different structures, storage conditions, and post processes were tested. As a result, our proposed model showed a nice correlation between predicted CA from chemical components and measured CA.

Keywords: wettability; ps laser; XPS; multiple regression analysis; surface functionalization;

1. Introduction

Recently, controlling the wettability of stainless steel surface by laser process has been studied by many researchers (Guan et al., 2015; Ngo and Chun, 2017; Pou et al., 2019; Sciancalepore et al., 2018). One of the

* Corresponding author. Tel.: +49 (0)631-415 575 19; fax: +49 (0)631-415 575 10
E-mail address: munehiro.chijiwa@pzkl.de

demands for the wettability of material surfaces from industrial applications is the long-term stability of wettability. However, a phenomenon that CA of water at laser micro-structured surface change over time (Kietzig et al., 2009) has been reported. Therefore, there is a challenge in understanding the mechanism of the change of CA at laser micro-structured surfaces over time.

It is widely known that CA depends on the physical (topography) and chemical properties of the surface. Moreover, several researchers showed that the topography of the laser microstructured surface is not changed over time. (Kietzig et al., 2009; Ngo and Chun, 2017) Therefore, the change of chemical properties over time is considered as the reason for the change of CA at laser micro-structured surface over time.

Despite various studies in the wettability of stainless steel surfaces by laser micro-structuring, up to now, it is far from complete understanding about the effect of chemical properties on the change of CA at laser micro-structured surfaces over time. For example, *Kietzig et al.* created dual-scale roughness structures on surfaces by using fs-laser and measured CA of water for 30 days (Kietzig et al., 2009). They found that the CA of water changes over time, and the CA of water was correlated with the amount of carbon on the structured surfaces. On the other hand, *Pou et al.* textured lines on samples with different process gases (Pou et al., 2019). Since metal oxides and nitrides were able to increase the polar component of the surface energy, they used different ratios of oxygen and nitrogen on iron to investigate the influence on the CA of water. Thus, since many parameters were considered as reasons for different CA of water, it is far from complete understanding about even the relationship between CA and chemical components.

In this study, to investigate the change of CA over time at laser microstructured surface in future, as for the first step, the relationship between CA and chemical components was investigated. For this purpose, CA and the local surface chemistry at the ps-laser micromachined surface on stainless steel 304 were discussed by using a model description, based on a multiple regression analysis. The proposed model was verified by using experimental data on the wetting behavior of different kinds of liquid (water and diiodo-methane) and surface chemistry measured by XPS spectroscopy.

2. Construction of prediction model

The CA depends on the physical (topography) and chemical properties of the surface so that at first the model of the physical part will be described and next the model of chemical properties will be introduced. Regarding, the physical part of the surface, a laser microstructured surface has artificial roughness. In this case, the CA measured on a laser microstructured surface is different from the CA on a flat surface. Most descriptions of the CA on roughness surface are based on the Wenzel model (Wenzel, 1936) as shown in eq. 1, and the Cassie-Baxter model (Cassie and Baxter, 1944) as shown in eq. 2.

$$\cos \theta_w = r \cos \theta_0 \quad (1)$$

$$\cos \theta_{CB} = f(\cos \theta_0 + 1) - 1 \quad (2)$$

where θ_w and θ_{CB} are the CA for the Wenzel equation or Cassie-Baxter equation, respectively. θ_0 is the CA for flat surface, r is the structure parameter which indicates the increase of interfacial contact area compared to flat surface and f is the fraction of wetted area.

Regarding, the chemical properties of a surface, a laser microstructured surface has a chemically heterogeneous surface because of contaminations from ambient air or chemical components of composite material. However, up to now, there are only a few discussions on the relationship between CA and chemical components. Therefore, in our model, CA at the chemically heterogeneous surface was considered.

Concerning the equation of CA for chemically heterogeneous surfaces, Cassie's equation (Cassie, 1948), which is expressed as a weighted integral of the area ratio of chemical components as shown in eq. 3 was used, instead of using Young's equation since Young's equation is for the chemically homogeneous surface.

$$\sigma_L \cos \theta_{0c} = a_1(\sigma_{S1} - \sigma_{S1L}) + a_2(\sigma_{S2} - \sigma_{S2L}) + \dots \quad (3)$$

where θ_{0c} is the effective CA for a flat but chemically heterogeneous surface. θ_{0c} will be substituted for θ_0 in eq. 1 or eq. 2, when the surface is chemically heterogeneous. σ_{Si} or rather σ_{SiL} is the surface free energy (SFE) and interfacial tension for each chemical component, a_i is the area ratio of the surface. By summing up all a_i becomes 1.

Meanwhile, the values of σ_{Si} and σ_{SiL} in eq. 3 are difficult to get from the experiment. To describe the term of interfacial tension (σ_{SiL}) by the term of SFE of solid (σ_{Si}), the equations of adhesion force between liquid and solid are used. Especially, for chemically homogeneous surfaces, usually, Dupre's equation and Owen and Wendt's model (Owens and Wendt, 1969) are used. However, to consider the chemically heterogeneous surface, in our model, Dupre's equation was modified as shown in eq. 4, and Owen and Wendt's model was modified as shown in eq. 5, and eq. 6.

$$W_{Ai} = \sigma_{Si} + \sigma_L - \sigma_{SiL} \quad (4)$$

$$\sigma_i = \sigma_i^D + \sigma_i^P \quad (5)$$

$$W_{Ac} = \sum_i^n a_i W_{Ai} = \sum_i^n 2a_i \left(\sqrt{\sigma_{Si}^D \sigma_L^D} + \sqrt{\sigma_{Si}^P \sigma_L^P} \right) \quad (6)$$

where W_{Ai} is the adhesion-force for each chemical component. σ_i , σ_i^D , σ_i^P are the total SFE and the dispersive part and polar part of the SFE, respectively. The index i numbers the chemical components. W_{Ac} is the effective adhesive force, σ_{Si}^D , σ_{Si}^P are the dispersive part and polar part of SFE for solid of each chemical component, respectively. σ_L^D and σ_L^P are the dispersive part and polar part of the SFE of the liquid.

From eq. 3 and eq. 4, the effective CA is expressed by the term of adhesion force and SFE of liquid. From eq. 6, the term of adhesion force is expressed by the dispersive and polar part of SFE. In the end, the relationship between the effective CA and the effect of chemical components is expressed as eq. 7 to eq. 9.

$$\frac{\sigma_L (\cos \theta_{0c} + 1)}{2\sqrt{\sigma_L^D}} = \sum_i^n a_i \sqrt{\sigma_{Si}^P} \frac{\sqrt{\sigma_L^P}}{\sqrt{\sigma_L^D}} + \sum_i^n a_i \sqrt{\sigma_{Si}^D} \quad (7)$$

$$A_m \equiv \sum_i^n a_i \sqrt{\sigma_{Si}^P} \quad (8)$$

$$B_m \equiv \sum_i^n a_i \sqrt{\sigma_{Si}^D} \quad (9)$$

A_m and B_m show the coefficient of polar part and dispersive part of solid. In eq. 7 to eq. 9, parameters of chemical components of material surface are expressed in A_m , B_m , a_i , and square roots of SFE of solid.

To predict CA from chemical components by using this model, A_m , B_m , a_i and square roots of SFE of solid are need to evaluate.

The value of A_m and B_m can be obtained from measuring the CA of different kinds of liquids on laser microstructured surfaces, and calculating effective CA from eq. 1 or eq. 2. It is because the dispersive and polar parts of SFE of some liquids are already known. (e.g. dispersive and polar part of water are 21.8 mN/m, 51.0 mN/m, dispersive and polar part of diiodo-methane are 50.8 mN/m, 0 mN/m).

The values of a_i can be obtained from measuring the concentrations of chemical components in the surface by XPS spectroscopy.

However, the values of square roots of the particular SFEs for solid are difficult to get from experiments. Therefore, another approach is needed. Since A_m and B_m can be expressed as a linear sum of the square roots of the particular SFEs for solid, we used a multiple regression analysis to approximate square roots of the particular SFEs for solid. For multiple regression analysis, the equation of residual squared sum was used as shown in eq. 10 and eq. 11.

$$S^P = \sum_j^k \left(A_{m(j)} - \left(a_{1(j)} \sqrt{\sigma_{s1}^P} + a_{2(j)} \sqrt{\sigma_{s2}^P} + \dots + a_{n(j)} \sqrt{\sigma_{sn}^P} \right) \right)^2 \quad (10)$$

$$S^D = \sum_j^k \left(B_{m(j)} - \left(a_{1(j)} \sqrt{\sigma_{s1}^D} + a_{2(j)} \sqrt{\sigma_{s2}^D} + \dots + a_{n(j)} \sqrt{\sigma_{sn}^D} \right) \right)^2 \quad (11)$$

Where S^P , S^D are the polar and dispersive parts of the residual squared sum. The indicator j shows the number of the experimental data set.

To get the approximate value of the square roots of the particular SFEs, a partial differentiates of the residual squared sum with respect to each square root of the particular SFEs is required to be small as shown in eq. 12 and eq. 13.

$$\frac{\partial S^P}{\partial \sqrt{\sigma_{Si}^P}} = 0 \quad (12)$$

$$\frac{\partial S^D}{\partial \sqrt{\sigma_{Si}^D}} = 0 \quad (13)$$

Then, to obtain approximate square roots of SFE, simultaneous equations of partial differentiation of residual squared sum need to be solved.

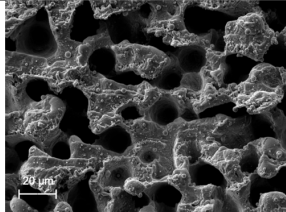
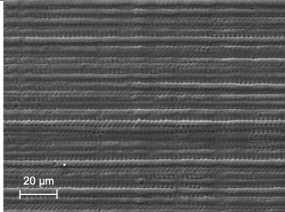
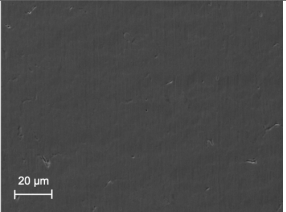
In the end, once the approximate value of square roots of SFE is obtained, CA at laser micro-structured surface will be predicted by using the concentrations of chemical components. This model will be discussed by using actual experiment data in the following sections.

3. Experiment

In this study, stainless steel sheets (SUS 304L, Hans-Erich Gemmel & Co. GmbH) with a dimension of 50 x 50 mm² and thickness of 1 mm were used. The surfaces were polished to optical quality (mirror polished surface). To reduce contaminations from the air on the sample, every sample was cleaned with isopropanol in an ultrasonic bath for 15 minutes and rinsed with distilled water before the laser process. The samples were micro-structured with an USP laser (Hyper-Rapid 25, Coherent Kaiserslautern GmbH) with a pulse duration of 10 ps and a wavelength of 532 nm. The laser system was integrated into a high-precision 5-axes micromachining workstation equipped with a galvanometric scanner system. For the experiments, a telecentric F-Theta optic with a focal length of 100 mm was used, resulting in a spot diameter of 10.2 μm. The laser processing was done in ambient air. The dimension of the micro-structured area was 10 x 10 mm².

For considering the topography effect, two different rough structures were created on the surface. The sponge-like structures, which have high roughness, were created. This kind of structure is known for getting super-hydrophobic for several days after the laser process (Sciancalepore et al., 2018). As for another structure, small roughness structures were created on stainless steel. As the CA on a rough surface is related to the CA on a flat surface via the structure parameter r and fraction f , according to eq. 1 and eq. 2, the surface topographies had to be determined for further quantitative analysis. To get reliable experimental data an Atomic Force Microscopy (Dimension 3100, Veeco Instruments. Inc) was used to determine the structure parameter for the laser micro-structured surfaces. From these measurements, a three-dimensional data set of the topography was obtained. From this data set, the surface area including the inside surface of cavities was calculated to obtain r , which is the value of surface area divided by flat area. Moreover, the data set was used to measure the local high area to derive f . For the un-microstructured surface (hereinafter called reference surface), a confocal microscope (Zeiss smart proof 5, Carl Zeiss AG) was used to determine the arithmetic mean roughness ($Ra = 0.03 \mu\text{m}$) and the mean width of the roughness profile ($RSm = 20 \mu\text{m}$). From these values, the structure parameter r for the reference surface is calculated. The morphologies of the microstructured surface in comparison to the reference surface, the experimental conditions, and structure parameter r and fraction f were summarized in table 1.

Table 1. Summary of structure and experimental condition and structure parameter.

	sponge-like structure	small roughness structure	reference
SEM			
laser power	9.6W	1.7W	/
pulse repetition rate	500KHz	200KHz	/
burst pulse	1	10	/
pulse overlap	75%	94%	/
hatching distance	5 μm	2.5 μm	/
scan times	16	8	/
r	1.42	1.10	1.00
f	0.2	/	/

For considering the chemical properties effect, different post processes and storage conditions were examined, since several researchers showed (Kietzig et al., 2009; Rajab et al., 2019) the different post-processes lead to different CA of water, which means different chemical properties. In this study, 2 different post processes and 2 different storage conditions for each structure were examined.

At first, all samples were cleaned with air blow just after the laser process and covered in Al foil to prevent contamination in the air, since some research (Giannuzzi et al., 2019) showed the change of CA by time is related to the increase of hydrocarbon. This hydrocarbon might come from contamination from air. For different post-process, since some research (Rajab et al., 2019) showed that when the stainless steel sample was boiled, CA of water kept low degree for a long-term, therefore some of the samples were unpacked from Al foil and boiled in hot distilled water for 8 hours, then covered in Al foil again. And some of the samples were

not boiled and kept in Al foil. For different storage conditions, some of the samples were unpacked from Al foil just 1 hour before XPS spectroscopy and stored in ambient air condition for 1 hour. Others were covered in Al foil. The summary of the post-process and storage conditions of samples is shown in table 2. In the end, in this study, 12 different kinds of the area were prepared. Each area has a different combination of structures and chemical components.

Table 2. Summary of sample number and experimental condition.

No.	post process	Store conditions
No.1	Air blow	Al foil
No.2	Air blow	ambient air
No.3	boiling	Al foil
No.4	boiling	ambient air

Hereafter, to conduct multiple regression analysis, a_i , A_m , B_m , in eq. 7 to 9 were examined.

To get a_i for all surfaces, which means evaluating the behavior of the chemical components of the surfaces, XPS spectroscopy was performed on the laser micro-structured area as well as on the reference surface. The surface chemistry was characterized by XPS (Axis Nova, Kratos Analytical. Ltd./ GB) after the laser process. The working pressure was lower than 10^{-8} mbar in the analyzing chamber. During the XPS analysis, the samples were stored on average inside the vacuum chamber of the XPS spectrometer chamber for 24 hours. From the peak area of photoelectron lines, relative concentrations of the elemental species at the surface were determined. In this measurement, carbon, oxygen, nitrogen, chromium, iron, calcium, magnesium, nickel, and silicon were detected at the sample surface. In addition, different chemical binding states of the dominant elements like carbon, oxygen, nitrogen, chromium, iron were identified via the chemical shift of their most prominent photoelectron line by high-resolution core-level spectra. By a detailed deconvolution of the atomic lines, quantitative ratios of the contributing chemical binding states were derived. In Table 3, the employed electron binding energies for the chemical binding states of detected elements are summarized.

Table 3. Used electron binding energies for the deconvolution of atomic core level spectra, according different chemical binding states.(Beamson et al., 2000; Moulder and Chastain, 1992)

elements	electron binding energies	chemical binding states
Carbon C1s	285.0eV	C-C(C-H)
	286.5eV	COC
	288.5eV	O=C-O, O-C-O
Oxygen O1s	530eV	FeO, Fe ₂ O ₃ , CrO ₃
	531.5eV	Org. O*=C-O, Cr ₂ O ₃
	532.8eV	Org. C-O, C-OH, O=C-O*
Nitrogen N1s	369.8eV	Metal Nitrides
	400eV	C-N, C-NH ₂
Chromium Cr2p	574eV	Metal
	577eV	Cr ₂ O ₃
	579eV	CrO ₃
Iron Fe2p	707eV	Metal
	709.4eV - 710.8eV	Oxide

For the multiple regression analysis, only elements relevant at the surface were considered. So metallic bulk material or trace elements with very small concentrations were neglected for the multiple regression

analysis. After omitting the bulk-specific metal components, to get representative concentrations for the sample surface, the sum of concentrations for all surfaces relevant species were normalized to 100%. Moreover, to avoid multicollinearity in the multiple regression analysis, some of the surface concentrations which are correlated by the chemical binding situation were omitted. In this study, among correlated concentrations, one of fewer correlation coefficients regard to A_m or B_m were omitted. In the end, chemical components of carbon-(C-C(C-H)), oxide-(layer), chromium oxide-(Cr_2O_3), and iron oxide were used in multiple regression analyses as shown in table 4. In table 4, nitrogen, calcium, magnesium, nickel, and silicon are not shown, since these elements are either metallic or trace elements.

Table 4. Summary of the elements for multiple regression analysis after considering metallic bulk material, trace elements and multicollinearity.

elements	binding states	reason for omitting	indication at this paper
carbon	C-C(C-H)	/	carbon-(C-C(C-H))
carbon	COC,O=C-O,O-C-O	multicollinearity	/
oxygen	FeO, Fe ₂ O ₃ , CrO ₃	multicollinearity	/
oxygen	Org. O=C-O, C-O, C-OH, Cr ₂ O ₃	/	oxygen-(layer)
chromium	Cr metal	metallic bulk material	/
chromium	Cr ₂ O ₃	/	chromium oxide-(Cr ₂ O ₃)
chromium	CrO ₃	trace elements	/
iron	iron Metal	metallic bulk material	/
iron	iron Oxid	/	Iron oxide

The concentrations of these components for each condition are summarized in fig. 1. According to fig.1, there was the trend that oxygen-(layer) at boiled samples has a high value compared to the sample without boiling. In addition, iron oxide at the reference surface was lower than iron oxide at the laser processed surface.

Next, to get A_m , B_m , in eq. 8, eq. 9, the CA for different kinds of liquid were measured after XPS spectroscopy by a drop shape analyzer device (DSA30, Krüss GmbH) with the liquid of droplet of 4 μl . In this study, water and diiodo-methane were used. It was due to that the dispersive and polar part of SFE of water and diiodo-methane were already known. (e.g. dispersive and polar part of water are 21.8 mN/m and 51.0 mN/m, dispersive and polar part of diiodo-methane are 50.8 mN/m, 0 mN/m). The results are shown in fig. 2. According to fig. 2, the CA for the water of boiled samples had a low CA of water compare to the samples without boiling. The CA for the water of sponge-like structures was larger than the small roughness structures in the same experiment condition.

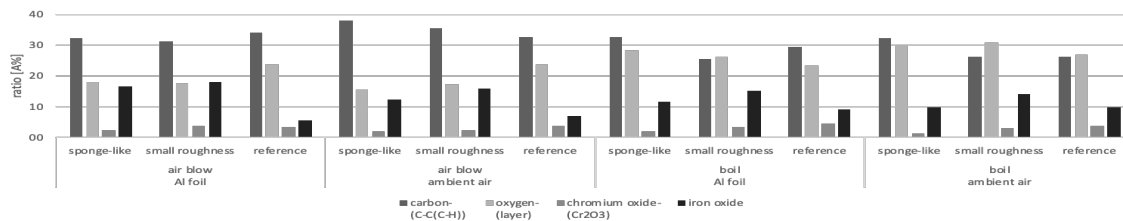


Fig. 1 The concentration of components used for multiple regression analysis for different experimental conditions.

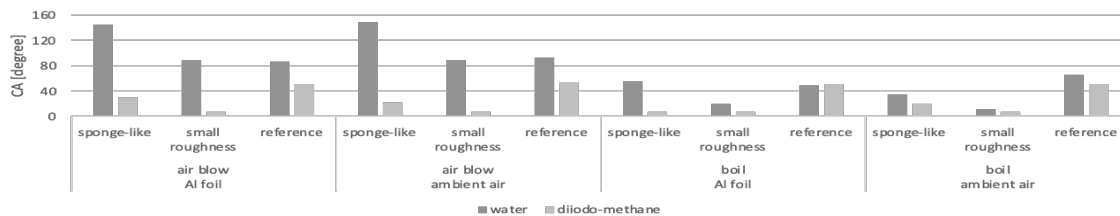


Fig. 2 The CA for water and diiodo-methane for different experimental conditions.

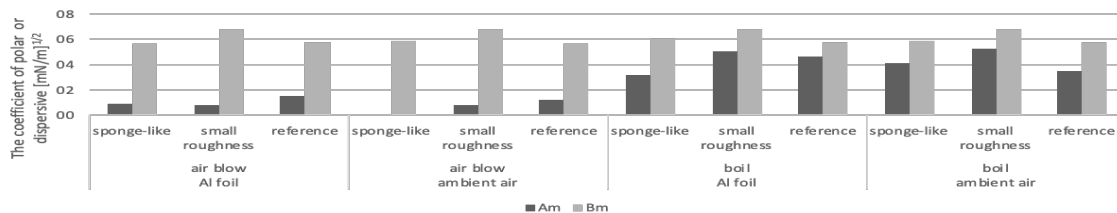


Fig. 3 The coefficient of polar and dispersive (A_m , B_m) for different experimental conditions.

By using these results of the CA and eq. 1, eq. 2 and eq. 7, the value of A_m and B_m , were obtained for the different structured surfaces and storage conditions or rather post processes. The results are shown in fig. 3. According to fig. 3, the results show that A_m at boiled samples had a high value compared to the samples without boiling. On the dispersive part B_m , there was a trend that small roughness was larger than sponge-like, and sponge-like was larger than reference.

These results showed that 12 data set which has different chemical properties were prepared by changing structure, post-processes and storage conditions.

4. Multiple regression analysis

By measuring the surface chemistries by XPS as well as CA for water and diiodo-methane, the values for A_m , B_m , and α_i in eq. 10 and eq. 11 were obtained. We were interested in the SFE of each chemical. To obtain the SFE for the polar part and dispersive part for our model, we used multiple regression analysis.

The prepared data set were used for the multiple regression analysis. While conducting multiple regression analysis, to eliminate the effect of randomness, the backward elimination method was used. This means starting with all candidate variables, and delete the variable if any whose loss gives the most statistically insignificant deterioration of the model fit. In this study, variables that showed a negative correlation coefficient and whose P-value was larger than 5% were both deleted. This process was repeated until no further variables were able to be deleted without a statistically insignificant loss of fit.

Table 5 shows the results of the multiple regression analysis. The chemical components column shows the intercept and kinds of chemical components which remained after multiple regression analysis. The coefficients column shows the intercept value and the coefficient value of each chemical component. The standard error column shows the standard deviation value of each chemical component in the model. For the coefficient of the polar part (A_m), the adjusted R square was 0.59. The value of R square shows how well the results were replicated by the model. When this value is closer to 1, this model is well described. oxygen-(layer) had a very low P-value (1.6%), which means this chemical well correlates to A_m . From these results, A_m

might correlate to polar chemical binding states of organics such as C-O, C-OH, and O=C-O. Other chemical components in the data set did not appear on this multiple regression analysis results, it might be because that effect of other chemical components was small compare to oxygen-(layer) or because the effect of chemical was random or the data set was not so enough for predicting the effect of the other parameter for this time.

Table 5. (a) SFE of polar part of each chemical components

chemical components	coefficients mN/m	standard error mN/m
Intercept	-29.0	22.1
oxygen-(layer)	1202.0	590.0

(b) SFE of dispersive part of each chemical components.

chemical components	coefficients mN/m	standard error mN/m
Intercept	23.9	1.8
iron oxide	131.9	32.9

For the coefficient value of the dispersive part (B_m), the adjusted R square was 0.86. Iron oxide had a very low P-value (0.06%), which means this chemical well correlates to B_m . Other chemical components did not appear on this multiple regression analysis results, it might be because the effect of other chemical component was small compare to iron oxide or because the effect of chemical was random or the data set was not so enough for predicting the effect of the other parameter for this time.

To verify this model, the CA of water and diiodo-methane were calculated from the concentrations of chemical components by using this model. These calculated CA were compared to the measured CA of water or diiodo-methane. The results are shown in fig. 4. According to fig. 4, this model showed a nice correlation between measured CA and calculated CA for small roughness structure and the reference surface. On the other hand, the sponge-like structure had less correlation. A significant challenge is the exact determination of the structure parameter for the sponge-like structure, due to the deterministic character of the surface. So, this value provides a big uncertainty and is part of a more detailed investigation in future experiments. Moreover, the standard deviation values of the difference between measured CA and calculated CA were calculated both for water and diiodo-methane. When this deviation for diiodo-methane was compared to the one of water, the deviation for diiodo-methane (9.1 degrees which are shown in the dashed line in fig. 4b) was less than the one of water (14.1 degrees which are shown in the dashed line in fig. 4a). This means the dispersive part of SFEs were predicted well since diiodo-methane has only dispersive part of SFE. On the other hand, the polar part of SFE is part of a more detailed investigation in future experiments. Furthermore, the change of chemical components by time will be investigated in the future by using this model.

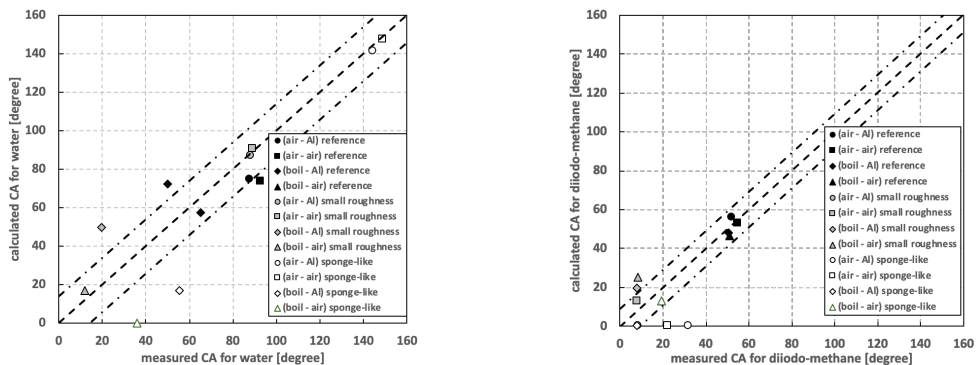


Fig. 4. (a) Comparison of measured CA and calculated CA (a) for water (b) for diiodo-methane

5. Conclusion

In this study, the relationship between CA and chemical components was investigated. For this purpose, the CA and the local surface chemistry at the ps-laser micromachined surface on stainless steel 304 were discussed by using a model description, based on a multiple regression analysis. The proposed model was verified by using experimental data on the wetting behavior of different kinds of liquid (water and diiodo-methane) and surface chemistry measured by XPS spectroscopy. As shown in multiple regression analysis, the polar part had a good correlation between oxygen-(layer), and the dispersive part had a good correlation between iron oxide. The comparison between measured CA for water and diiodo-methane, and calculated CA for water and diiodo-methane from multiple regression analysis results had a good correlation between them for small roughness surface and the reference surface.

Acknowledgements

This project was supported by the “Bundesministerium für Wirtschaft und Energie (BMWi)” under the program “Zentrales Innovationsprogramm Mittelstand (ZIM)” with the project number “ZF4058606PK8”.

The authors wish to thank for Prof. Dr. Peter Starke (Hochschule Kaiserslautern) for lending us confocal microscope and Prof. Dr. Egbert Oesterschulze (Technische Universität Kaiserslautern) for lending us atomic force microscope.

References

- G. Beamson, D. Briggs, and SurfaceSpectra Ltd., “The XPS of polymers database.” SurfaceSpectra, Manchester, 2000.
- A. B. D. Cassie, “Contact angles,” *Discuss. Faraday Soc.*, vol. 3, no. 0, pp. 11–16, Jan. 1948.
- G. Giannuzzi et al., “Short and long term surface chemistry and wetting behaviour of stainless steel with 1D and 2D periodic structures induced by bursts of femtosecond laser pulses,” *Appl. Surf. Sci.*, vol. 494, pp. 1055–1065, Nov. 2019.
- Y. C. Guan, F. F. Luo, G. C. Lim, M. H. Hong, H. Y. Zheng, and B. Qi, “Fabrication of metallic surfaces with long-term superhydrophilic property using one-stop laser method,” *Mater. Des.*, vol. 78, pp. 19–24, Aug. 2015.
- A.-M. Kietzig, S. G. Hatzikiriakos, and P. Englezos, “Patterned Superhydrophobic Metallic Surfaces,” *Langmuir*, vol. 25, no. 8, pp. 4821–4827, Apr. 2009.
- J. F. Moulder and J. Chastain, *Handbook of X-ray Photoelectron Spectroscopy: A Reference Book of Standard Spectra for Identification and Interpretation of XPS Data*.
- C.-V. Ngo and D.-M. Chun, “Fast wettability transition from hydrophilic to superhydrophobic laser-textured stainless steel surfaces under low-temperature annealing,” *Appl. Surf. Sci.*, vol. 409, pp. 232–240, Jul. 2017.
- D. K. Owens and R. C. Wendt, “Estimation of the surface free energy of polymers,” *J. Appl. Polym. Sci.*, vol. 13, no. 8, pp. 1741–1747, 1969.
- P. Pou et al., “Laser texturing of stainless steel under different processing atmospheres: From superhydrophilic to superhydrophobic surfaces,” *Appl. Surf. Sci.*, vol. 475, pp. 896–905, May 2019.
- F. H. Rajab, Z. Liu, and L. Li, “Long term superhydrophobic and hybrid superhydrophobic/superhydrophilic surfaces produced by laser surface micro/nano surface structuring,” *Appl. Surf. Sci.*, vol. 466, pp. 808–821, Feb. 2019.
- C. Sciancalepore, L. Gemini, L. Romoli, and F. Bondioli, “Study of the wettability behavior of stainless steel surfaces after ultrafast laser texturing,” *Surf. Coat. Technol.*, vol. 352, pp. 370–377, Oct. 2018.